

Coherence properties of the two-dimensional Bose-Einstein condensate

Christopher Gies* and D. A. W. Hutchinson†

Department of Physics, University of Otago, P.O. Box 56, Dunedin, New Zealand

We present a detailed finite-temperature Hartree-Fock-Bogoliubov (HFB) treatment of the two-dimensional trapped Bose gas. We highlight the numerical methods required to obtain solutions to the HFB equations within the Popov approximation, the derivation of which we outline. This method has previously been applied successfully to the three-dimensional case and we focus on the unique features of the system which are due to its reduced dimensionality. These can be found in the spectrum of low-lying excitations and in the coherence properties. We calculate the Bragg response and the coherence length within the condensate in analogy with experiments performed in the quasi-one-dimensional regime [Richard *et al.*, Phys. Rev. Lett. **91**, 010405 (2003)] and compare to results calculated for the one-dimensional case. We then make predictions for the experimental observation of the quasicondensate phase via Bragg spectroscopy in the quasi-two-dimensional regime.

PACS numbers: 03.75.Hh, 05.30.Jp, 67.40.Db

I. INTRODUCTION

Bose-Einstein condensation (BEC) in (quasi-) two-dimensional systems has only recently been obtained in the laboratory [1, 2]. Thus, many properties have yet to be explored both experimentally and theoretically. We present an investigation of an isotropic two-dimensional BEC with the aim of providing detailed predictions for comparison with future experiments.

The manner in which dimensionality can fundamentally alter the physics of a system is clearly apparent in the Mermin-Wagner-Hohenberg theorem, which forbids a spontaneously broken symmetry with long range order in a homogeneous two-dimensional system [3–5]. In terms of the coherence function $G^{(1)}(\mathbf{x}, \mathbf{x}')$, this means that $\lim_{|\mathbf{x}-\mathbf{x}'|\rightarrow\infty} G^{(1)}(\mathbf{x}, \mathbf{x}') \neq 0$, which can be seen as the definition of BEC [6, 7], is impossible for $T > 0$ in a uniform two-dimensional system. Thus, in a two-dimensional Bose gas BEC cannot occur at finite temperatures. Phase fluctuations make the formation of a globally coherent phase impossible. Despite this, a different transition of the Kosterlitz-Thouless (KT) type [8–10] to a state with an analytical decay in the coherence function is possible in the ideal system.

With confinement in a harmonic trap, the modified density of states allows the 2D system to Bose condense. Nevertheless, below the critical temperature there is a large phase fluctuating regime in which the superfluid is best described as a quasicondensate [11]. Unlike a true BEC, phase coherence only extends over regions of a size smaller than the extent of the condensate, characterized by the coherence length. This regime has been referred to as the KT phase, although the physical state of the interacting system in this phase fluctuating regime has yet to be thoroughly investigated. Phase fluctuations can enter the uniform gas in the form of vortex/antivortex

pairs, or topological charges, which unbind at the point of the KT transition. Thus, the phase fluctuating state may well be a regular lattice of pairs of opposite topological charges in the sense of the KT phase, but this is not the only possibility and further investigation is required.

In a previous publication [12] we have discussed how the semi-classical approximation fails to describe BEC consistently in two dimensions and have shown results to prove that these problems can be removed by applying the more complex Hartree-Fock-Bogoliubov (HFB) formalism. The aim of the present publication is to present a detailed and more complete discussion of the properties of a two-dimensional BEC as is possible within the HFB-Popov approach. Our emphasis lies on the coherence properties which are crucial for the question of whether the superfluid state is best described as a BEC or as a quasicondensate. In the following section we outline the HFB formalism and explain our methods of obtaining solutions. Then, in Section III, we present our results, such as the density profile of the condensate and non-condensate, the excitation spectrum and the coherence function. In Section III C we present the momentum profile and coherence length of a phase fluctuating condensate, indicating how these could be measured in forthcoming experiments. Our work is concluded in Section IV.

II. FORMALISM

A. Mean-field theory and HFB-Popov equations

The time-independent, second quantized form of the grand-canonical many-body Hamiltonian operator for our system is given by

$$\hat{H} = \int d^2r \hat{\psi}^\dagger(\mathbf{r}) \left(\hat{h}(\mathbf{r}) - \mu \right) \hat{\psi}(\mathbf{r}) + \frac{g}{2} \int d^2r \hat{\psi}^\dagger(\mathbf{r}) \hat{\psi}^\dagger(\mathbf{r}) \hat{\psi}(\mathbf{r}) \hat{\psi}(\mathbf{r}) . \quad (1)$$

*Electronic address: cluso@physics.otago.ac.nz

†Electronic address: hutch@physics.otago.ac.nz

Here, $\hat{h}(\mathbf{r}) = -\frac{\hbar^2}{2m}\Delta + U_{\text{trap}}(\mathbf{r})$ is the single particle Hamiltonian with the external potential U_{trap} of the atom trap, and g is the coupling parameter that characterizes interparticle scattering. For collision processes, we assume a hard sphere potential within the usual pseudo-potential approximation [13], i. e. $V(\mathbf{r} - \mathbf{r}') = g\delta^{(2)}(\mathbf{r} - \mathbf{r}')$. For a dilute gas this is a good approximation, however care must be taken in determining the coupling constant g . Usually it is derived from an approximation to the two-body T-matrix in the zero-energy and zero-momentum limit, as appropriate for scattering processes in an ultra-cold system. In three dimensions, the two-body T-matrix for a dilute gas is well described within the s-wave approximation, $g = 4\pi\hbar^2 a_{3D}/m$, where a_{3D} is the s-wave scattering length. In two dimensions, however, the two-body T-matrix vanishes at zero energy [14]. Therefore, many-body effects introduced by the surrounding medium must be taken into account when studying two-dimensional gases. For a trapped gas, this leads to a spatially dependent coupling parameter $g(\mathbf{r})$. Furthermore, the exact form of the coupling strength depends on the tightness of the confinement in the axial direction. With the parameters from [1], using the terminology of [14], we consider this system to be in the quasi-2D regime. Therefore, for the calculations undertaken in this work, we use the following approximation to the many-body T-matrix at zero temperature for the coupling parameter [14]:

$$g(\mathbf{r}) = -\frac{4\pi\hbar}{m} \frac{1}{\ln(n_c(\mathbf{r})g(\mathbf{r})ma_{2D}^2/4\hbar^2)}. \quad (2)$$

The scattering length a_{2D} in the quasi-2D regime is given by $a_{2D} = 4\sqrt{\pi/B}l_z e^{-\sqrt{\pi}l_z/a_{3D}}$, $B \approx 0.915$. This result was first obtained by Petrov *et al.* [15, 16] by considering the 2D scattering problem. We will present a detailed study of interactions in the 2D Bose condensed system elsewhere [17].

We decompose the Bose field operators, in the standard fashion [18, 19], into classical and fluctuation parts, $\hat{\psi}(\mathbf{r}) \simeq \langle \hat{\psi}(\mathbf{r}) \rangle + \delta\hat{\psi}(\mathbf{r}) = \Psi_0(\mathbf{r}) + \delta\hat{\psi}(\mathbf{r})$, where the condensate wave function $\Psi_0(\mathbf{r})$ is normalized to the number of particles in the ground state, i. e. $\int d^2r |\Psi_0(\mathbf{r})|^2 = N_0$. The Hamiltonian (1) can then be diagonalized by a unitary transformation to the quasiparticle operators $\hat{\alpha}_i, \hat{\alpha}_i^\dagger$, $\delta\hat{\psi}(\mathbf{r}) = \sum_i (\hat{\alpha}_i u_i(\mathbf{r}) - \hat{\alpha}_i^\dagger v_i^*(\mathbf{r}))$, yielding the HFB-Hamiltonian

$$\begin{aligned} \hat{H}_{\text{HFB}} = & \int d^2r \Psi_0(\mathbf{r}) \left(\hat{h}(\mathbf{r}) - \mu + \frac{1}{2}g(\mathbf{r})n_c(\mathbf{r}) \right) \Psi_0(\mathbf{r}) \\ & + \sum_i E_i \hat{\alpha}_i^\dagger \hat{\alpha}_i - C \end{aligned} \quad (3)$$

where $\hat{\mathcal{L}} = \hat{h}(\mathbf{r}) - \mu + 2g(\mathbf{r})n(\mathbf{r})$ and $n_c(\mathbf{r})$, $\tilde{n}(\mathbf{r})$ and $n(\mathbf{r}) = n_c(\mathbf{r}) + \tilde{n}(\mathbf{r})$ are the condensate, non-condensate and total densities, respectively. The functions u_i, v_i are referred to as quasiparticle amplitudes, and E_i are the

quasiparticle energies. The first term in (3) is the condensate part and merely a c -number. The second term is the Hamiltonian for non-interacting quasiparticles and is formally equivalent to the case of the harmonic oscillator. The constant energy shift C arises from the Bogoliubov transformation [18] and from terms left over from the quartet operator averages of the fluctuation operators which are factorized in a fashion analogous to Wick's theorem [20, §4.2]. However, this energy shift has no impact on the solution of the HFB equations.

The form (3) of the Hamiltonian requires that the order parameter obeys the generalized Gross-Pitaevskii equation (GPE)

$$\left(\hat{h}(\mathbf{r}) - \mu \right) \Psi_0(\mathbf{r}) + g(\mathbf{r}) (n_c(\mathbf{r}) + 2\tilde{n}(\mathbf{r})) \Psi_0(\mathbf{r}) = 0 \quad (4)$$

and that the quasiparticle amplitudes and energies obey the coupled Bogoliubov-de Gennes (BdG) equations

$$\begin{aligned} \hat{\mathcal{L}} u_i(\mathbf{r}) - g(\mathbf{r}) \Psi_0(\mathbf{r})^2 v_i(\mathbf{r}) &= E_i u_i(\mathbf{r}) \\ \hat{\mathcal{L}} v_i(\mathbf{r}) - g(\mathbf{r}) \Psi_0^*(\mathbf{r})^2 u_i(\mathbf{r}) &= -E_i v_i(\mathbf{r}), \end{aligned} \quad (5)$$

so as to eliminate off-diagonal terms in the quasiparticle field operators. The BdG equations determine the elementary excitation modes of the condensate. We refer to (4), together with (5), as the HFB equations. Note that we have taken the Popov approximation by neglecting the anomalous average of the fluctuation operator, $\tilde{m}(\mathbf{r}) = \langle \delta\hat{\psi}(\mathbf{r})\delta\hat{\psi}(\mathbf{r}) \rangle$, whereby avoiding divergence problems of this quantity and the occurrence of a gap in the excitations spectrum [18, 19]. Once the BdG equations are solved, the non-condensate density $\tilde{n} = \langle \delta\hat{\psi}^\dagger(\mathbf{r})\delta\hat{\psi}(\mathbf{r}) \rangle$ can be obtained by populating the quasiparticle states,

$$\tilde{n}(\mathbf{r}) = \sum_i f_B(E_i) (|u_i(\mathbf{r})|^2 + |v_i(\mathbf{r})|^2) + |v_i(\mathbf{r})|^2, \quad (6)$$

where the quasiparticle distribution function with the inverse temperature β is given by

$$f_B(E_i) = \langle \hat{\alpha}_i^\dagger \hat{\alpha}_i \rangle = \frac{1}{z^{-1}e^{\beta E_i} - 1}. \quad (7)$$

Here, the fugacity z is determined by the difference between the chemical potential μ and the condensate eigenvalue λ , $z = e^{\beta(\mu-\lambda)}$, since the quasiparticle energies are measured relative to the condensate [20]. To a good approximation, we can use the result for the non-interacting gas, i. e.

$$z^{-1} = 1 + \frac{1}{N_0}. \quad (8)$$

The system we consider has a finite number of atoms. The fugacity fulfills the practical purpose of preventing the number of thermal atoms from exceeding the total atom number and, hence, the condensate density from becoming negative in our numerical calculations.

In order to study coherence properties, we calculate the normalized first order correlation, or coherence function, which can be written in terms of the field operators as [21]

$$g^{(1)}(\mathbf{r}, \mathbf{r}') = \frac{\langle \hat{\psi}^\dagger(\mathbf{r}) \hat{\psi}(\mathbf{r}') \rangle}{\sqrt{\langle \hat{\psi}^\dagger(\mathbf{r}) \hat{\psi}(\mathbf{r}) \rangle \langle \hat{\psi}^\dagger(\mathbf{r}') \hat{\psi}(\mathbf{r}') \rangle}} . \quad (9)$$

Given the decomposition of the field operator, the coherence function can be expressed in terms of the off-diagonal densities

$$n_c(\mathbf{r}, \mathbf{r}') = \Psi_0^*(\mathbf{r}) \Psi_0(\mathbf{r}') \quad (10)$$

$$\tilde{n}(\mathbf{r}, \mathbf{r}') = \langle \delta \hat{\psi}^\dagger(\mathbf{r}) \delta \hat{\psi}(\mathbf{r}') \rangle . \quad (11)$$

The latter can be calculated from the off-diagonal version of (6). Using the above for the correlation function, (9) gives

$$g^{(1)}(\mathbf{r}, \mathbf{r}') = \frac{n_c(\mathbf{r}, \mathbf{r}') + \tilde{n}(\mathbf{r}, \mathbf{r}')}{\sqrt{n(\mathbf{r}) n(\mathbf{r}')}} . \quad (12)$$

The correlation function is related to the momentum spectrum of the condensate by a simple Fourier transformation, i. e.

$$n(\mathbf{k}) = \langle \hat{\phi}^\dagger(\mathbf{k}) \hat{\phi}(\mathbf{k}) \rangle = \int d^2r d^2r' e^{i\mathbf{k} \cdot (\mathbf{r} - \mathbf{r}')} \langle \hat{\psi}^\dagger(\mathbf{r}) \hat{\psi}(\mathbf{r}') \rangle , \quad (13)$$

with $\hat{\phi}(\mathbf{k})$ and $\hat{\phi}^\dagger(\mathbf{k})$ being the field operators in momentum space. This implies that coherence properties can be directly measured in an experiment, as has been done in [22] for the quasi-one-dimensional case by means of Bragg spectroscopy. In a Bragg experiment, the propagation speed of the light field is determined by the detuning of the crossed laser beams [23]. Therefore, the spectral response of the condensate is measured as a function of the detuning. To establish the relationship with the momentum distribution, we use the relation between the detuning δ and the momentum within the condensate plane p_\perp for a n -photon process,

$$\delta = \frac{n k_L p_\perp}{2\pi m} , \quad (14)$$

where $k_L = 2\pi/\lambda$, λ is the wavelength of the light field (780.02 nm for Rubidium [22], 589 nm for Sodium [24]), and m the mass of the atoms.

B. Numerical Methods

We discuss some aspects important to the solution of the finite temperature HFB equations. The trapping frequency in the axial direction is sufficiently large so that the dynamics in this dimension are frozen out ($\hbar\omega_z > k_B T$). In the radial plane, we consider an isotropic trapping potential with the radial frequency

ω_\perp , $U_{\text{trap}} = m\omega_\perp^2 r^2/2$. Thus, our system is cylindrically symmetric and we can effectively treat the problem as one-dimensional upon changing to cylindrical coordinates. We scale all equations to computational units, i. e. lengths by the oscillator length, $a_0 = \sqrt{\hbar/m\omega_\perp}$, and energies by the Rydberg of energy, $E_0 = \hbar\omega_\perp/2$.

The calculation follows a self-consistent, iterative scheme, as proposed in [18]. First, the GPE is solved with the non-condensate density set to zero. Taking this calculated condensate density, the BdG equations are solved to obtain the quasiparticle modes. These are then populated through the quasiparticle distribution function (7), with the sum of all the excited particles yielding the thermal density. With the non-condensate density now known, we go back and solve the generalized GPE and the whole process is repeated until convergence.

To begin, we expand the order parameter in a set of basis states. A convenient basis for this problem is given by the eigenstates of the 2D harmonic oscillator, since the single-particle Hamiltonian is diagonal in this basis. To take the cylindrical symmetry into account, we write the eigenfunctions of the oscillator problem $\hat{h}_{\text{osc}} = -\Delta + r^2$ in terms of the Laguerre polynomials L_n^m ,

$$\chi_{n,m}(r, \varphi) = \frac{1}{\sqrt{\pi} \Gamma(1+m) \binom{n+m}{n}} r^m e^{-r^2/2 + im\varphi} L_n^m(r^2) , \quad (15)$$

with the eigenenergies $E_{n,m} = 2(2n+m+1)$. The quantum number m defines the angular momentum. Since the condensate ground state has zero angular momentum, for the solution of the GPE merely the $m=0$ subspace must be considered. In order to numerically solve the GPE, we use an optimization routine with a Thomas-Fermi profile as the initial guess.

The solution of the BdG equations follows the method described in [19]. In a first step, the BdG equations (5) are decoupled by a transformation to the auxiliary functions $\psi_i^{(\pm)}(r) = u_i(r) \pm v_i(r)$. Omitting spatial dependencies, this leads to

$$\begin{aligned} (\hat{h}_{\text{GF}} - \mu)^2 \psi_i^{(+)} + 2gn_c(\hat{h}_{\text{GF}} - \mu) \psi_i^{(+)} &= E_i^2 \psi_i^{(+)} \\ (\hat{h}_{\text{GF}} - \mu)^2 \psi_i^{(-)} + 2g(\hat{h}_{\text{GF}} - \mu) n_c \psi_i^{(-)} &= E_i^2 \psi_i^{(-)} , \end{aligned} \quad (16)$$

where $\hat{h}_{\text{GF}} \equiv \hat{h} + g(n_c + 2\tilde{n})$ is the Hamiltonian in the generalized GPE (4). The auxiliary functions $\psi_i^{(\pm)}(r)$ are then expanded in the basis set in which \hat{h}_{GF} is diagonal. This basis we term the Hartree-Fock (HF) basis and it is obtained by the full solution of the generalized GPE, i. e.

$$(\hat{h}_{\text{GF}} - \mu) \phi_\alpha(r) = \varepsilon_\alpha \phi_\alpha(r) , \quad (17)$$

where $\{\phi_\alpha(r)\}$ is the HF basis. The primary advantage of this basis is that all excited states are by definition orthogonal to the condensate, after the lowest momentum state, which is the condensate state itself, has been removed from the basis set. Both the calculation of the

HF basis, as well as the solution of the decoupled BdG equations are only linear problems, since the condensate density is given from the solution of the GPE, and can be solved in a straightforward manner. The eigenvalue problem corresponding to the BdG equations is block-diagonal with no overlap between the subspaces of different angular momentum, so that the solution to (16) can be obtained separately in each subspace. The thermal density then follows from (6) by summing up the contributions from all angular momentum subspaces.

Naturally, the number of basis states used in the discrete, quantum mechanical calculation is limited by an upper energy cutoff, ϵ_{cut} , which must be introduced consistently in all angular momentum subspaces. To account for the contributions above the energy cutoff, we use the semi-classical approximation [25, 26], so that

$$\tilde{n}(r) = \sum_i \tilde{n}_i^{\text{qm}}(r) \times \Theta(\epsilon_{\text{cut}} - E_i) + \int_{\epsilon_{\text{cut}}}^{\infty} dE \tilde{n}^{\text{sc}}(E, r). \quad (18)$$

The contribution $\tilde{n}_i^{\text{qm}}(r)$ below the cutoff is given by the addend in (6), and above the cutoff by the semi-classical equation, with the Heaviside function Θ , and again omitting spatial dependencies,

$$\tilde{n}^{\text{sc}} = \frac{m}{2\pi\hbar^2} \left\{ f_B(E) + \frac{1}{2} - \frac{E}{2\sqrt{E^2 + (gn_c)^2}} \right. \\ \left. \times \Theta \left(E - \sqrt{(U_{\text{trap}} - \mu + 2gn)^2 - (gn_c)^2} \right) \right\}. \quad (19)$$

III. RESULTS

We will now present the results of our numerical calculation. We consider a sample of 2000 sodium atoms that are trapped in a harmonic potential with the parameters of the experiment by Görlitz *et al.* [1]. The radial trapping frequency is $\omega_{\perp} = 2\pi \times 790$ Hz. Unless otherwise stated, all quantities are expressed in dimensionless form.

A. Thermal density and condensate population

1. Density profiles

Figure 1 shows the thermal density at different temperatures. The temperature dependent term in (6) leads to the formation of the characteristic off-center peak of the non-condensate density. It is located at the edge of the condensate due to the repulsion of the thermal atoms by the condensate. This is depicted in Figure 2, where the two densities n_c and \tilde{n} are plotted together. In comparison to the rapidly decaying condensate density, the thermal density has a long tail. Thus, the condensate is

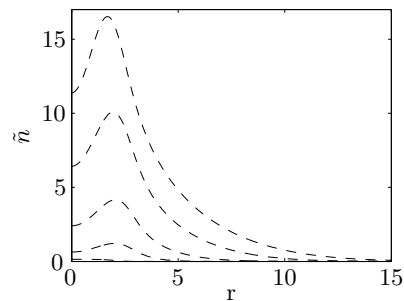


FIG. 1: Non-condensate density at $T/T_c = 0, 0.1, 0.25, 0.5$ and 0.75 (from bottom to top). The lowest line corresponds to the quantum depletion.

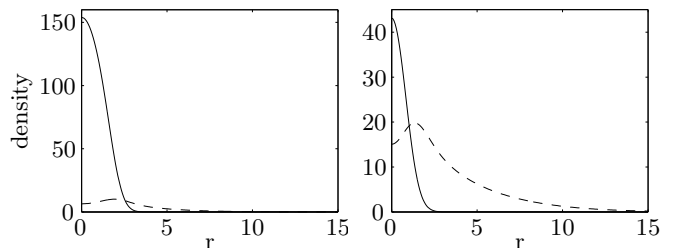


FIG. 2: Condensate (solid) and non-condensate density (dashed) at 0.5 and $0.9 T_c$.

relatively dense with a sharp peak within the diffuse thermal cloud. The tail of the thermal cloud becomes longer as the temperature increases, while the condensate radius does not change significantly even if the number of condensate atoms drops by an order of magnitude. Note that the long tail contains a large number of atoms despite its low density because the spatial integral is weighted by a factor of r (r^2 in three dimensions). The slight change in the size of the condensate can also be seen in the shift of the non-condensate peak towards the trap center with increasing temperature, remaining located at the edge of the condensate. Note that even at zero temperature there is a small fraction of excited atoms due to the temperature-independent quantum depletion term in (6).

From the existence of a well defined condensate and non-condensate density we can already infer coherence information. Following the argument in [12, 16], a measure of phase fluctuations is given by $\langle \hat{\delta}^2 \rangle \approx \tilde{n}/n_c$, where $\hat{\delta}$ is the phase fluctuation operator in the alternative decomposition $\hat{\psi}(r) \simeq \sqrt{\tilde{n}(r)} e^{i\hat{\delta}(r)}$. Phase fluctuations become important when $\langle \hat{\delta}^2 \rangle \gtrsim 1$. Thus, as long as $n_c > \tilde{n}$, these fluctuations are suppressed in the system.

2. Ground state population

In Figure 3 the condensate population is shown as a function of temperature. The results are compared to the case of the trapped ideal gas, where the population

is determined by a power law expression. We fit the following functional form to the numerical data:

$$\frac{N_0}{N} = 1 - \left(\frac{T}{\bar{T}_c}\right)^\beta, \quad \text{where } \bar{T}_c = \alpha T_c. \quad (20)$$

In the case of the ideal gas, $\beta = 2$ and $\alpha = 1$. In the fit the critical temperature is reduced by a factor of about 5% with $\alpha \approx 0.95$. This shift has two contributions: The finite size of the system reduces the critical temperature [27], but it is also modified by the interactions. This second contribution as been extensively discussed in the literature, see the recent publication [28] and references therein. For the exponent we find $\beta \approx 1.70$, which is 15% smaller than for the ideal trapped gas. With these values, (20) parameterizes our data very well except near the critical temperature, where finite size effects are significant and the exact method of determining the shift of the chemical potential from the condensate eigenvalue becomes important. In the ideal gas the chemical po-

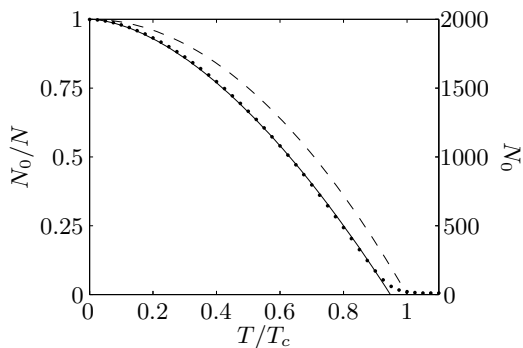


FIG. 3: Condensate population versus temperature. The solid line corresponds to a fit to (20), the dashed line shows the ideal gas power law dependence. The points are results from the HFB-Popov calculation.

tential is zero at the point of the phase transition, and therefore the transition point is strictly defined. In the interacting gas, the chemical potential depends implicitly on the non-condensate [19] and, when this becomes large, the transition point becomes smeared out. Technically, the occurrence of the finite temperature tail can be explained through the fugacity term in the quasiparticle distribution function (7), which is explicitly given by (8). The term $\propto 1/N_0$ prevents the condensate population from becoming negative. However, this expression for the fugacity is only approximate and the shape of the tail and the speed with which it approaches zero depends on the explicit choice of the fugacity term at temperatures around \bar{T}_c .

B. Condensate excitations

The low-lying collective or elementary excitation modes of the condensate, determined by the solution of the BdG equations, are of interest because they reflect

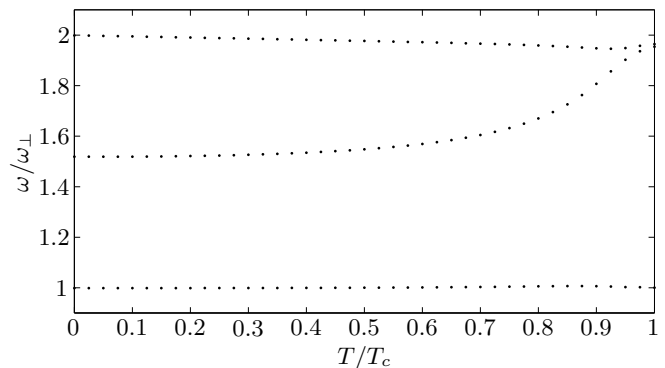


FIG. 4: Low-lying excitation modes of the condensate as a function of temperature. The uppermost line corresponds to the *breathing mode* with angular momentum quantum number $m = 0$, the middle line to the *quadrupole mode* with $m = 2$. The lowest line is the *Kohn mode*, $m = 1$, which lies constantly at the trapping frequency.

certain fundamental symmetry properties of the system, as well as being easily accessible to experiments.

Figure 4 shows the modes with angular momentum $m = 0, 1, 2$ as a function of temperature. Each of the three branches corresponds to the lowest quasiparticle energy eigenvalue in the lowest three, separated, angular momentum subspaces, in which the BdG equations are solved, c. f. Section II B.

a. Breathing mode. The breathing mode corresponds to an oscillation of the condensate radius and lies at a frequency that is twice the trapping frequency. As shown in [29], this is due to a hidden symmetry of the many-body Hamiltonian with a $\delta^{(2)}$ -interaction potential and a harmonic trapping potential in two dimensions. As the temperature increases, the non-condensate density grows and starts to constitute a deviation from the harmonic oscillator potential in the effective potential of the Gross-Pitaevskiĭ equation, so that the frequency shifts slightly from $2\omega_\perp$. The effective potential is weakened by the presence of the static thermal atoms so that the frequency decreases. If the dynamics of the thermal cloud were included in the calculation [30], then the full symmetry of the Hamiltonian would be restored and the mode frequency would remain precisely at $2\hbar\omega_\perp$.

b. Kohn mode. The Kohn mode corresponds to a center of mass oscillation of the whole condensate. Less effected by the perturbation to the harmonic potential of the static thermal cloud, it remains very constant at the trapping frequency, as is predicted by the generalized Kohn theorem [31]. However, looking closer at Figure 4, one may see a slight increase in the frequency near the critical temperature as the effective potential becomes less harmonic and, therefore, breaks the Kohn theorem. In our calculation we treat the thermal cloud as stationary. An inclusion of the full dynamics of the thermal cloud would, again, ensure the Kohn mode remains constant at all temperatures [19, 30, 32].

c. Quadrupole mode. The quadrupole mode is the only low-lying mode which depends strongly upon the temperature. The frequency of this mode could thus, in principle, be used as a measure of the temperature of the 2D gas.

With increasing temperature, all three frequencies smoothly approach the frequencies of the non-interacting gas and the breathing and quadrupole mode become degenerate. Using a local density approximation with the relation $\mu = g[n_c(r) + 2\tilde{n}(r)]$ for the uniform gas in the Hartree-Fock approximation [33, §8.3], it is easy to show that the BdG equations for $n_c(r) = 0$, given by

$$\left(\hat{h}(r) - \mu + 2g\tilde{n}(r) - E_i\right) u_i(r) = 0, \quad (21)$$

recover the energies of the harmonic oscillator. In the case that there is still a condensate, the total density in the region where $n_c(r) \neq 0$ is approximately constant just below the critical temperature, so that the mean-field energy only constitutes a near constant shift to the trapping potential and, hence, only slightly alters the eigenfrequencies of the trap.

We would briefly like to draw comparison with the three-dimensional case where the frequency spectrum looks very similar [19, 34]. The striking difference is the breathing mode which is temperature dependent in three dimensions, whereas it is a feature of the two-dimensional system to have breathing oscillations with a universal energy of $2\hbar\omega_{\perp}$.

C. Coherence properties

1. Correlation function

a. Interacting gas. In Figure 5 the correlation function $g^{(1)}(0, r)$ is depicted at various temperatures. The r -axis has been scaled by the size of the condensate. This is not the Thomas-Fermi radius, but we choose a minimal allowed condensate density in such a way that the whole condensate at zero temperature is phase coherent.

The decay of the correlation function allows for a characterization of the gaseous system. At low temperatures the correlation function has a constant value throughout the extent of the condensate, indicating a truly coherent Bose-Einstein condensed phase with off-diagonal long-range order. Algebraic decay is associated with the KT phase and, at intermediate temperatures, the superfluid must be identified as a quasicondensate. At very high temperatures, clearly visible for the highest temperature in Figure 5, the coherence function decays exponentially, showing that long-range order is lost completely.

At very low temperatures the correlation functions show some unphysical oscillations that are purely numerical noise. At low temperatures $n(r) \approx n_c(r)$. In the limit $\tilde{n} \equiv 0$ the correlation function (9) is given by the Heaviside function $\Theta(1 - r/r_{\text{con}})$. However, there is a small contribution from the quantum depletion of the

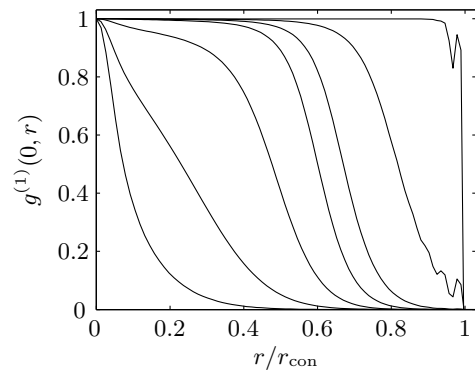


FIG. 5: Correlation function $g^{(1)}$ for the non-interacting Bose gas at different temperatures T/T_c : 0, 0.025, 0.05, 0.1, 0.5, 0.9 and 1 from right to left.

condensate that smoothes the sharp corner as $g^{(1)}$ drops to zero, causing a loss of numerical accuracy as we divide two very similar small numbers in (12).

The coherence length can be extracted by measuring the full width at half maximum (fwhm) of $g^{(1)}$ and is shown in Figure 8.

b. Non-interacting gas. The off-diagonal density matrix is known in closed analytical form for the non-interacting gas. It can be determined by means of the inverse Laplace transform of the zero-temperature Bloch density matrix [35, 36]. Its explicit form in two dimensions at temperature T is given by

$$g^{(1)}(\mathbf{r}, \mathbf{r}', T) = \sum_{j=1}^{\infty} \frac{e^{j\mu/T}}{\pi(1 - e^{-2j/T})} \times \exp\left(-\frac{|\mathbf{r} + \mathbf{r}'|^2}{4} \tanh(j/2T) - \frac{|\mathbf{r} - \mathbf{r}'|^2}{4} \coth(j/2T)\right). \quad (22)$$

We find the chemical potential $\mu = \mu(T)$ for the trapped non-interacting gas by solving $\sum_{n=0}^{\infty} f_B(E_n = n + 1, \mu, T) (n + 1) - N = 0$ with respect to μ . Here, $f_B = [(1 + N_0^{-1})e^{\beta(E_n - \mu)} - 1]^{-1}$ is the Bose-Einstein distribution function *with the fugacity factor* (8) that takes into account the number of condensate particles from the HFB calculation. Without this fugacity factor, finite size effects, taken into account in the HFB calculation, would be neglected and, therefore, the comparison would be between two approaches based on different assumptions. The expression (22) for the correlation function is exact at all temperatures. Numerically, the infinite sum can be calculated up to any required accuracy.

We compared our code against these exact results for the non-interacting gas. At all temperatures the HFB results agree perfectly with the correlation function calculated from (22), implying that the numerics works well even at high temperatures. Deviations would indicate an insufficiency in the basis set or inaccuracy due to an insufficient fineness or range of the computational grid.

The influence of the interactions can be seen in Figure

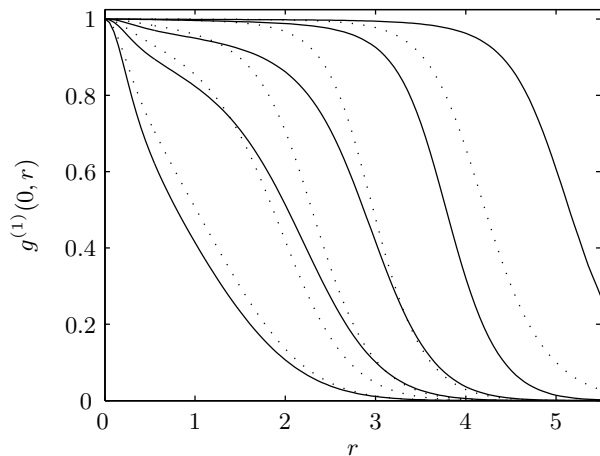


FIG. 6: Correlation function $g^{(1)}$ for the non-interacting Bose gas at different temperatures T/T_c : 0.025, 0.1, 0.5, 0.8 and 0.95 from right to left. The solid lines correspond to the HFB-Popov results for the interacting gas, the dotted lines represent the exact result for the non-interacting gas (22).

6. The solid lines show the coherence function for the interacting gas, compared to the exact non-interacting gas equation, shown as dotted lines. We see that interactions increase the coherence length in a large part of the temperature regime. At $0.8T_c$ and above, however, the coherence length of the interacting gas is decreased relative to the non-interacting gas. This can be explained by the effect of the mean-field interaction on the condensate radius. At high temperatures (N_c small) the radius of the interacting condensate is approximately the same as the radius of the non-interacting condensate, given by the size of the lowest harmonic oscillator state. At low temperatures, however, the condensate population is large and mean-field effects broaden the condensate. Correspondingly, the coherence function of the interacting condensate is broader. If the spatial coordinate was scaled by the size of the condensate as in Figure 5, the plot would show that interactions always reduce the range of coherence.

2. Momentum spectrum

Figure 7 shows the momentum spectrum corresponding to (13), as it could be measured by means of Bragg spectroscopy. It has been calculated by Fourier transforming the correlation function shown in Figure 5. On the ordinate is the detuning of the Bragg laser beams, which is directly proportional to the momentum of the atoms, c.f. (14). The highest peak corresponds to the lowest temperature where the momentum distribution of the atoms is narrowest. With increasing temperature the spectrum is broadened. An experimental setup is limited by its resolution at low temperatures, because of the decrease of the spectral width.

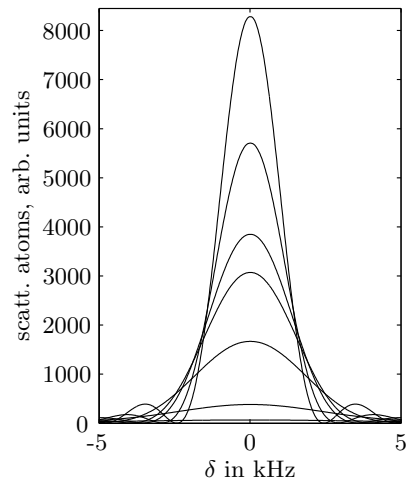


FIG. 7: Momentum spectrum, with intensity corresponding to the fraction of scattered atoms as function of the Bragg detuning δ . Temperatures T/T_c from top: 0, 0.025, 0.05, 0.1, 0.5, 0.9 and 1.

In Figure 8, the coherence length obtained from the momentum spectra in Figure 7 is plotted. We determine the coherence length by fitting the momentum profile and measuring the half width of the fit. A Gaussian provides a good fit at temperatures $\lesssim 0.9T_c$. Above a small crossover regime, the momentum profiles at temperatures higher than $0.925T_c$ fit more closely to a Lorentzian. Thus, the data points in Figure 8 correspond to the fwhm of a Gaussian or a Lorentzian fit, depending on which gives better agreement with the data.

In the same graph the lengths are compared to those obtained from the results shown in Figure 5. Qualitatively the results agree with each other, although those obtained from $g^{(1)}$ lead to somewhat smaller values for the coherence length. Also one can see that the extracted half widths of the correlation function are subject to a slight inaccuracy, whereas the widths calculated from the fits to the momentum profile result in a smooth line over the whole temperature regime. Note that the coherence length is to some extent a matter of personal definition, as e.g. we could have chosen $1/e$ rather than the fwhm.

Looking at the decay of the coherence length in Figure 8, we can distinguish three different regimes. Close to zero temperature, the slope is very steep and the coherence length decreases to a third of the condensate size by about $0.1T_c$. Then, up to about $0.8T_c$, l_ϕ decreases monotonically, but much more slowly. From there up to the critical temperature, the coherence length again drops rapidly.

A decreasing coherence length directly implies a loss in the global phase coherence of the superfluid phase. A true Bose-Einstein condensate cannot be said to exist when the phase of the order parameter fluctuates on a length scale significantly smaller than the extent of the condensate. At this point we should instead refer to a quasicondensate. From Figure 5 we see that the coher-

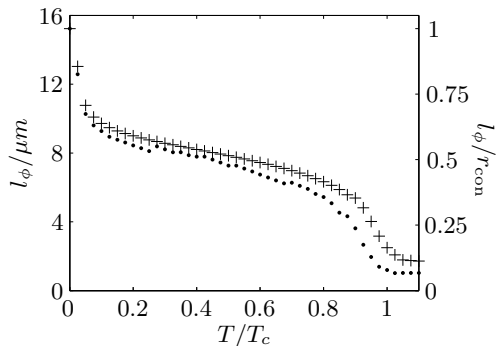


FIG. 8: Coherence length of the condensate, shown in both real units and scaled by the extension of the condensate. The upper line (+) has been calculated from the momentum spectrum (left panel), the lower line (·) is the data from Figure 5.

ence length drops smoothly. Therefore, it is difficult to determine an exact point on the temperature scale where the transition from a true condensate to a quasicondensate takes place. At about $0.5 T_c$ the coherence length has dropped to about half of the maximal value. The maximal value we can use to determine the spatial extent of the condensate, indicated on the right axis in Figure 8. The treatment in [16] predicts a value of approximately $0.4 T_c$ for our parameters for phase fluctuations to become dominant. Our result is, therefore, consistent with [16], although the coherent phase seems to persist at slightly higher temperatures.

3. Comparison to 1D

Similar behaviour has been observed in calculations for the one-dimensional Bose gas at finite temperatures [37]. Looking at the coherence function presented by Ghosh, we see that in the one-dimensional case the coherence length drops even more rapidly than in the two-dimensional case, showing that phase fluctuations become much more dominant as the dimension is reduced further. In 1D, the temperature range between 0.3 and $0.5 T_c$ has about the same coherence properties as the range around $0.9 T_c$ in our 2D calculation. Ghosh identifies the 1D phase at temperatures as low as $0.1 T_c$ as a quasicondensate with large phase fluctuations. From an examination of Figure 5, we see that, at this temperature in the 2D case, even if the coherence length has decreased slightly, there is still a large proportion of the condensate where $g^{(1)}$ is constantly 1, indicating that the system is essentially a phase coherent BEC.

In 1D the Lorentzian momentum profile has been found to be characteristic of the phase-fluctuating quasicondensate [38] and has been used as an identifying signature of such a phase [22]. However,

we are convinced that the shape change we observe is not a signature of a phase fluctuating condensate, but the effect of the fugacity term as N_0 goes to zero. Furthermore, from looking at the correlation function in Figure 5, we would expect the phase fluctuations to become important, indicating the presence of a quasicondensate, at about $0.5 T_c$, long before the momentum profile becomes Lorentzian in character.

IV. CONCLUSION

We have used the HFB formalism to investigate the finite-temperature physics of a Bose-Einstein condensate confined to a two-dimensional geometry. Unlike the three dimensional case, phase fluctuations must be taken into consideration at comparatively lower temperatures. In a regime below the critical temperature they destroy the global coherence of the condensate and the superfluid state is best described as a quasicondensate. In the HFB formalism phase fluctuations are included via the contribution to the non-condensate density from low-energy quasiparticles. We have shown that the formalism is not only applicable in the strictly phase coherent regime, but also that the quantities obtained, such as the single-particle off-diagonal density matrix, allow for a quantitative analysis even in the phase fluctuating regime. Our work is consistent with [16], although we find that, within the HFB treatment, the pure condensate phase persists to higher temperatures.

The coherence length of the condensate can be determined from its correlation function or the momentum profile. Following Aspect *et al.* for the one-dimensional case [22, 39], we have calculated the Bragg spectrum for a condensate in two dimensions. We found the values extracted for the coherence length to be in qualitative agreement with those calculated for the one-dimensional Bose gas, although a true BEC with global phase coherence still exists at much higher temperatures than in the 1D case. The Bragg spectrum provides a clear signature of the quasicondensate phase and we anticipate experimental efforts in this area in the near future.

Acknowledgments

The authors would like to acknowledge financial support from the Marsden and ISAT Linhages Funds of the Royal Society of New Zealand, as well as a University of Otago Research Grant. We thank Sam Morgan, Mark Lee and Brandon van Zyl for many useful conversations during various exchange visits and subsequently.

-
- [1] A. Görlitz, J. M. Vogels, A. E. Leanhardt, C. Raman, T. L. Gustavson, J. R. Abo-Shaeer, A. P. Chikkatur, S. Gupta, S. Inouye, T. Rosenband, et al., *Phys. Lett.* **87**, 130402 (2001).
- [2] D. Rychtarik, B. Engeser, H.-C. Nägerl, and R. Grimm, *Phys. Rev. Lett.* **92**, 173003 (2004).
- [3] N. D. Mermin and H. Wagner, *Phys. Rev. Lett.* **17**, 1133 (1966).
- [4] N. D. Mermin, *Phys. Rev.* **176**, 250 (1968).
- [5] P. C. Hohenberg, *Phys. Rev.* **158**, 383 (1967).
- [6] O. Penrose and L. Onsager, *Phys. Rev.* **104**, 576 (1956).
- [7] C. N. Yang, *Rev. Mod. Phys.* **34**, 694 (1962).
- [8] J. M. Kosterlitz and D. J. Thouless, *J. Phys. C: Solid State Phys.* **6**, 1181 (1973).
- [9] J. M. Kosterlitz, *J. Phys. C: Solid State Phys.* **7**, 1046 (1974).
- [10] V. L. Berezinski, *Sov. Pys. JETP* **32** (1971), [*Zh. Eksp. Teor. Fiz.* **59**, 907 (1970)].
- [11] V. N. Popov, *Functional Integrals in Quantum Field Theory and Statistical Physics* (D. Reidel Publishing Company, Holland, 1983).
- [12] C. Gies, B. P. van Zyl, S. A. Morgan, and D. A. W. Hutchinson, *Phys. Rev. A* **69**, 023616 (2004).
- [13] K. Huang, *Statistical Mechanics* (John Wiley & Sons, New York, 1987), 2nd ed.
- [14] M. D. Lee, S. A. Morgan, M. J. Davis, and K. Burnett, *Phys. Rev. A* **65**, 043617 (2002).
- [15] D. S. Petrov and G. V. Shlyapnikov, *Phys. Rev. A* **64**, 012706 (2001).
- [16] D. S. Petrov, M. Holzmann, and G. V. Shlyapnikov, *Phys. Rev. Lett.* **84**, 2551 (2000).
- [17] C. Gies, M. D. Lee, and D. A. W. Hutchinson, *to be published*.
- [18] A. Griffin, *Phys. Rev. B* **53**, 9341 (1996).
- [19] D. A. W. Hutchinson, K. Burnett, R. J. Dodd, S. A. Morgan, M. Rusch, E. Zaremba, N. P. Proukakis, M. Edwards, and C. W. Clark, *J. Phys. B* **33**, 3825 (2000).
- [20] S. A. Morgan, *J. Phys. B* **33**, 3847 (2000).
- [21] M. Naraschewski and R. J. Glauber, *Phys. Rev. A* **59**, 4595 (1999).
- [22] S. Richard, F. Gerbier, J. H. Thywissen, M. Hugbart, P. Bouyer, and A. Aspect, *Phys. Rev. Lett.* **91**, 010405 (2003).
- [23] P. B. Blakie, R. J. Ballagh, and C. W. Gardiner, *Phys. Rev. A* **65**, 033602 (2002).
- [24] S. R. Wilkinson, C. F. Bharucha, K. W. Madison, Q. Niu, and M. G. Raizen, *Phys. Rev. Lett.* **76**, 4512 (1996).
- [25] J. Reidl, A. Csordás, R. Graham, and P. Szépfalussy, *Phys. Rev. A* **59**, 3816 (1999).
- [26] W. J. Mullin, *J. Low Temp. Phys.* **110**, 167 (1998).
- [27] S. Giorgini, L. P. Pitaevskii, and S. Stringari, *Phys. Rev. A* **54**, R4633 (1996).
- [28] B. Kastening, *Phys. Rev. A* **69**, 043613 (2004).
- [29] L. P. Pitaevskii and A. Rosch, *Phys. Rev. A* **55**, R853 (1997).
- [30] S. A. Morgan, M. Rusch, D. A. W. Hutchinson, and K. Burnett, *Phys. Rev. Lett.* **91**, 250403 (2003).
- [31] J. F. Dobson, *Phys. Rev. Lett.* **73**, 2244 (1994).
- [32] N. P. Proukakis, S. A. Morgan, S. Choi, and K. Burnett, *Phys. Rev. A* **58**, 2435 (1998).
- [33] C. J. Pethick and H. Smith, *Bose-Einstein Condensation in Dilute Gases* (Cambridge University Press, 2002).
- [34] D. A. W. Hutchinson, R. J. Dodd, and K. Burnett, *Phys. Rev. Lett.* **81**, 2198 (1998).
- [35] B. P. van Zyl, *Phys. Rev. A* **68**, 033601 (2003).
- [36] B. P. van Zyl, R. K. Bhaduri, A. Suzuki, and M. Brack, *Phys. Rev. A* **67**, 023609 (2003).
- [37] T. K. Ghosh, Preprint *cond-mat/0402079* (2004).
- [38] F. Gerbier, J. H. Thywissen, S. Richard, M. Hugbart, P. Bouyer, and A. Aspect, *Phys. Rev. A* **67**, 051602(R) (2003).
- [39] A. Aspect, S. Richard, F. Gerbier, M. Hugbart, J. Retter, J. Thywissen, and P. Bouyer, Proceedings of the International Conference on Laser Spectroscopy (ICOLS 03), Cairns, Australia (2003).